

Transport of organelles by elastically coupled motor proteins

Deepak Bhat^a and Manoj Gopalakrishnan

Department of Physics, Indian Institute of Technology Madras, Chennai 600036, India (e-mail: manojgopal@iitm.ac.in)

Received: date / Revised version: date

Abstract. Motor-driven intracellular transport is a complex phenomenon where multiple motor proteins simultaneously attached on to a cargo engage in pulling activity, often leading to tug-of-war, displaying bidirectional motion. However, most mathematical and computational models ignore the details of the motor-cargo interaction. A few studies have focused on more realistic models of cargo transport by including elastic motor-cargo coupling, but either restrict the number of motors and/or use purely phenomenological forms for force-dependent hopping rates. Here, we study a generic model in which N motors are elastically coupled to a cargo, which itself is subjected to thermal noise in the cytoplasm and to an additional external applied force. The motor-hopping rates are chosen to satisfy detailed balance with respect to the energy of elastic stretching. With these assumptions, an $(N + 1)$ - variable master equation is constructed for dynamics of the motor-cargo complex. By expanding the hopping rates to linear order in fluctuations in motor positions, we obtain a linear Fokker-Planck equation. The deterministic equations governing the average quantities are separated out and explicit analytical expressions are obtained for the mean velocity and diffusion coefficient of the cargo. We also study the statistical features of the force experienced by an individual motor and quantitatively characterize the load-sharing among the cargo-bound motors. The mean cargo velocity and the effective diffusion coefficient are found to be decreasing functions of the stiffness. While increase in the number of motors N does not increase the velocity substantially, it decreases the effective diffusion coefficient which falls as $1/N$ asymptotically. We further show that the cargo-bound motors share the force exerted on the cargo equally only in the limit of vanishing elastic stiffness; as stiffness is increased, deviations from equal load sharing are observed. Numerical simulations agree with our analytical results where expected. Interestingly, we find in simulations that the stall force of a cargo elastically coupled to motors is independent of the stiffness of the linkers.

PACS. 05.40.Fb random walks – 05.40.-a stochastic processes – 87.16.Nn motor proteins – 05.10.Gg Langevin method

1 Introduction

Motor-protein based cargo transport is a mechanism which governs the spatial organisation of organelles like endosome, vesicles, mitochondria etc. inside a eukaryotic cell. A few proteins belonging to dynein and kinesin families are known to be involved in transporting the cargoes on microtubule filaments [1,2,3]. Using the structural polarity of the microtubule, dyneins move toward the minus end of a microtubule, while most kinesins move toward the plus end [4]. In many cases, the cargo is driven by multiple motor proteins leading to increased stall force and transport over longer distances [5,6]. Due to the involvement both dyneins and kinesins, motion of cargo is found to be bidirectional in some cases [7,8]. Experiments have shown evidence for tug-of-war mediated mechanical interaction between two teams of opposing motors (dyneins and kinesins) leading to bidirectional motion of cargoes [9,10].

Mechanical interaction between motors of the same polarity is less understood.

A few experiments have given insights about the nature of interaction between multiple motor proteins by coupling them artificially through a DNA scaffold [11,12]. In [11], DNA coupled by two kinesins effectively behaved as though the single motor attachment state dominated the motility. This led to the conclusion that asynchronous stepping of kinesins show dominant negative interference. While the average velocity of the coupled system was almost same as that of single motor, the run length was observed to be much larger for coupled motors. In another interesting experiment reported in Furuta et al.[12], multiple motors were made to attach on a DNA scaffold with controlled separations between them. The velocity and the stall force of the DNA scaffold was found to be affected by changes in the spatial separation between the motors. These observations clearly indicate the presence of chemical or mechanical interaction between similar motors.

^a *Present address:* International Centre for Theoretical Sciences, Survey No. 151, Shivakote, Hesaraghatta Hobli, Bengaluru North 560089, India (e-mail:deepak.bhat@icts.res.in)

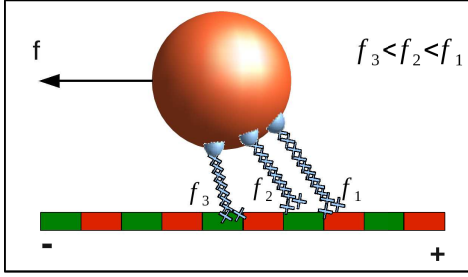


Fig. 1. The figure shows a set of motor proteins are pulling a cargo against an external load f . As each motor protein is at a different spatial separation from the cargo, individual motors experience different stretching forces. In particular, the leading motor experiences a large force and a lagging motor experience a smaller force.

Motor proteins and motor-driven membranous organelles like endosomes, mitochondria etc. are soft molecules with stiffness typically of the order of a few pNnm^{-1} [1, 13, 14]. Since motor proteins exert forces of a few pN on these organelles, the elastic nature of motor-cargo assembly is likely to be an influential factor in the transport process. Early models on unidirectional and bidirectional transport have generally ignored the details of interaction between similar motor proteins in a team [15, 16, 17, 18]. In these models, external force on the cargo is assumed to be shared equally among the like motors, akin to a “mean-field” approximation [19]. It is, however, plausible that stretching of the elastic motor-cargo linkers generates tension on the motors even in the absence of any external force on the cargo. Further, in the presence of external force, the force experienced by an individual motor could differ from the mean-field value. As depicted in fig.1, the elastic stretching force experienced by a motor on a cargo depends on its spatial location which changes with time, and is, therefore, a fluctuating quantity.

Several studies have appeared in the last few years, based (mostly) on Hookean spring-like interaction between motor and the cargo [19, 20, 21, 22, 23, 24, 25, 26, 27, 28, 29]. In Kunwar et al. [20], along with elastic interaction among the motors, non-linear force-velocity relations are assigned to different motors. Average run length of multiple motor driven cargo in the presence of external force is studied computationally at different motor stiffnesses. A more systematic semi-analytic study done by Materassi et al. [21] reproduced the results in [20]. It was shown by Kunwar et al. [19] that, compared to the mean-field model in which load is assumed to be shared equally among the motors of same directionality, a stochastic load sharing model based on elastic motor-cargo interaction can explain unidirectional transport more reliably. They found, however, that neither model is consistent with all the experimental observations of bidirectional transport. In a computational study, Bouzat and Falo [22] have shown that the stall force of the cargo-motor assembly is larger for non-interacting motors than motors interacting through elastic strain force. In another study by Bouzat and Falo [23], tug-of-war between multiple opposing motors is investi-

gated and it is shown that the mean velocity of the cargo is independent of the stiffness, whereas the mean runtime decreases with increase in stiffness. A discrete state transition rate model employed in [24] showed slight reduction in two motor run length and velocity at larger stiffnesses, due to increase in the strain force. In a more recent study, Berger et al. [25] identified four distinct transport regimes in a system of two elastically coupled motor proteins. In [28], the dynamics of the cargo coupled to a single motor protein was studied using a novel coarse-graining approach based on separation of time-scales between the cargo and motor. A very recent study by Bouzat [29] showed that a model in which motors experience history-dependent forces captures some of the experimental observations better than the previously studied models.

Some of the formalisms developed in the above mentioned analytical studies were applied to simple cases with at most two motor proteins driving a cargo [24, 25, 26, 28], while many other studies are by and large computational in nature [19, 20, 22, 23, 29]. A general theoretical framework to study the motion of a cargo driven by arbitrary number of elastically bound motors has not been developed. We develop such a treatment in this paper. We study the motion of a cargo pulled by N elastically coupled motor proteins in a viscous medium, subject to thermal noise and an external applied force. Starting from the complete master equation, we extract deterministic dynamical equations for the averages and a linear Fokker-Planck equation (LFPE) for the fluctuations. We study the effects of elastic stiffness and the number of motors on various statistical properties such as the drift and diffusion of the cargo, force experienced by each motor protein and its deviation from the mean field approximation. Finally, we carry out computer simulations in order to verify our analytical results and mostly observe good agreement between the two wherever expected. Among the limitations of our study, spontaneous and load-induced detachment of motors from the filament is completely neglected. Also, truncation of the expansion of the master equation leads to incorrect prediction on the variation of stall force with stiffness. These limitations will be partially addressed in a future publication.

The paper is organised as follows. In sec.2, we describe our model and set up the complete master equation, which is separated into deterministic “macroscopic” equations for the averages and a LFPE for fluctuations. We derive various properties of the cargo transport such as the average cargo velocity and effective diffusion coefficient of the motor-cargo complex in sec.2.1. One of the important ingredients in the model, the elastic stretching energy dependence of motor jumping rates, is discussed in sec.2.2. In sec.2.3, we apply the formalism developed in sec.2.1 to a cargo driven by N identical motors. In sec.2.4, we describe the computer simulations techniques employed in our study and in sec.2.5 we verify all the results obtained in sec.2.3 using computer simulations. We compare predictions of our model with experiments in sec.3. Finally, in sec.4 we summarize our results and discuss some of their implications.

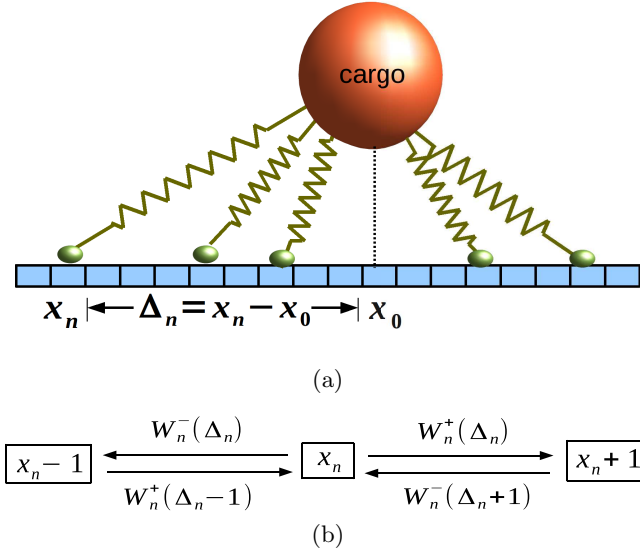


Fig. 2. (a) Cartoon of multiple elastic motor proteins (shown as springs) coupled to a cargo performing one-dimensional Brownian motion on a microtubule. (b) A motor at x_n jumps forward with a rate $W_n^+(\Delta_n)$ and backward with a rate $W_n^-(\Delta_n)$. The corresponding reverse transition rates, with starting points at $x_n + 1$ and $x_n - 1$ are, respectively, given by $W_n^-(\Delta_n + 1)$ and $W_n^+(\Delta_n - 1)$.

2 A generic model for a cargo elastically coupled to N motor proteins

A motor protein moving on a microtubule filament moves in a sequence of jumps of fixed length (usually, although dynein is known to take variable-sized jumps in response to load [30,31]) from one monomer to the next. For a single free motor protein, let ℓ be the jump length, w_n and v_n be the forward and backward hopping rates respectively. A motor protein is imagined to be bound to the cargo using a spring of stiffness κ_n , which is an approximation to the motor-cargo linker in our model. We consider a cargo pulled by N such motor proteins simultaneously, as depicted in fig.2(a). In reality, the stiffness κ_n could also have contribution from the elastic nature of membranous cargo, which we have not taken separately in to account. Let x_0 and x_n ($1 \leq n \leq N$) be the positions of the cargo and the n 'th motor on the filament respectively, expressed in units of jump length ℓ . For the sake of later convenience, we use the convention $\mathbf{x} \equiv \{x_0, x_1, \dots, x_N\}$. If $\Delta_n = x_n - x_0$ is the instantaneous separation between n 'th motor and the cargo, then the instantaneous elastic force on the n 'th motor is $f_n = -\ell\kappa_n\Delta_n$ and so the elastic force on the cargo due to all the motors at different locations on the filament is $f_c = \ell \sum_{i=1}^N \kappa_i \Delta_i$. For a cargo bound to N motor proteins and acted on by an external force f , the over-damped Langevin equation is written as [22,28]

$$\ell \dot{x}_0 = \ell \sum_{i=1}^N \frac{\kappa_i \Delta_i}{\gamma} + \frac{f}{\gamma} + \zeta(t), \quad (1)$$

where γ is the drag coefficient, $\zeta(t)$ is Gaussian white noise: $\langle \zeta(t) \rangle = 0$ and $\langle \zeta(t)\zeta(t') \rangle = D\delta(t - t')$, where $D = 2k_B T / \gamma$ following the fluctuation-dissipation theorem. Note that the sign of f is positive when the force acts in the $+x_0$ direction; hence an ‘‘opposing force’’ will have $-$ sign in this convention.

The hopping rates of the individual motors are modified by the presence of the elastic stretching energy. Let us denote by $W_n^+(\Delta_n)$ and $W_n^-(\Delta_n)$ the single motor hopping rates for the forward ($x_n \rightarrow x_n + 1$) and backward ($x_n \rightarrow x_n - 1$) transitions respectively, as shown in fig.2(b). Then, the complete equation for the probability distribution $P(\mathbf{x}; t)$, that describes the stochastic dynamics of the motor-cargo system is written as:

$$\frac{\partial P(\mathbf{x}; t)}{\partial t} = \sum_{n=1}^N [(\mathbb{E}_n^+ - 1)W_n^- P + (\mathbb{E}_n^- - 1)W_n^+ P] - \frac{\partial}{\partial x_0} \left[\left(\sum_{i=1}^N \frac{\kappa_i}{\gamma} \Delta_i + \frac{f}{\ell\gamma} \right) P - \left(\frac{D}{2\ell^2} \right) \frac{\partial P}{\partial x_0} \right] \quad (2)$$

where \mathbb{E}_n^+ and \mathbb{E}_n^- are a set of N raising and lowering operators, defined through the relations $\mathbb{E}_n^+ P(x_0, x_1, \dots, x_n, \dots) = P(x_0, x_1, \dots, x_n + 1, \dots)$, and similarly, $\mathbb{E}_n^- P(x_0, x_1, \dots, x_n, \dots) = P(x_0, x_1, \dots, x_n - 1, \dots)$ [32].

2.1 Expansion of the master equation

In eq.2, we expand all the variables x_n about their average values $\overline{x_n(t)}$ as follows:

$$x_n = \overline{x_n(t)} + \eta_n \quad 0 \leq n \leq N, \quad (3)$$

where η_n are fluctuations about the averages, hence $\langle \eta_n \rangle = 0$ by construction. The dynamics may be described now in terms of the variables η_n , the probability distribution of which is defined as $\Pi(\boldsymbol{\eta}; t) \equiv P(\mathbf{x}; t)$ so that

$$\frac{\partial P(\mathbf{x}; t)}{\partial t} = \frac{\partial \Pi(\boldsymbol{\eta}; t)}{\partial t} - \sum_{n=0}^N \frac{d\overline{x_n}}{dt} \frac{\partial \Pi}{\partial \eta_n}. \quad (4)$$

With the shift of variables in eq.3, the operators \mathbb{E}_n^+ and \mathbb{E}_n^- in eq.2 admit the Taylor expansion [32]

$$\mathbb{E}_n^\pm = \sum_{m=0}^{\infty} \frac{(\pm 1)^m}{m!} \frac{\partial^m}{\partial \eta_n^m}. \quad (5)$$

Insertion of eq.5 along with eq.4 into eq.2 yields the following Kramers-Moyal expansion in terms of the variables η_m :

$$\frac{\partial \Pi}{\partial t} - \sum_{n=0}^N \dot{\overline{x_n}} \frac{\partial \Pi}{\partial \eta_n} = \sum_{n=0}^N \sum_{m=1}^{\infty} \left[-\frac{1}{(2m-1)!} \frac{\partial^{2m-1}}{\partial \eta_n^{2m-1}} (V_n \Pi) + \frac{1}{(2m)!} \frac{\partial^{2m}}{\partial \eta_n^{2m}} (D_n \Pi) \right], \quad (6)$$

where

$$V_n = W_n^+ - W_n^- \quad ; \quad D_n = W_n^+ + W_n^-, \quad (7)$$

for $1 \leq n \leq N$, while

$$V_0 = \sum_{i=1}^N \frac{\kappa_i}{\gamma} \Delta_i + \frac{f}{\ell \gamma} \quad ; \quad D_0 = \frac{D}{\ell^2}. \quad (8)$$

To proceed further, we carry out Taylor expansion of V_n and D_n in powers of the fluctuations η_n , leading to

$$\begin{aligned} V_n(\mathbf{x}) &= \bar{V}_n + \sum_k \alpha_{nk}^{(1)} \eta_k + \sum_{k,l} \alpha_{nkl}^{(2)} \eta_k \eta_l + \dots \\ D_n(\mathbf{x}) &= \bar{D}_n + \sum_k \beta_{nk}^{(1)} \eta_k + \sum_{k,l} \beta_{nkl}^{(2)} \eta_k \eta_l + \dots \end{aligned} \quad (9)$$

where we have defined (a) the “macroscopic” variables

$$\bar{V}_n \equiv V_n(\bar{\mathbf{x}}) \quad ; \quad \bar{D}_n \equiv D_n(\bar{\mathbf{x}}) \quad (10)$$

and (b) Taylor coefficients of order r ($r \geq 1$)

$$\alpha_{nkl..}^{(r)} = \frac{1}{r!} \frac{\partial^r V_n}{\partial x_k \partial x_l \dots} \bigg|_{\mathbf{x}=\bar{\mathbf{x}}} \quad ; \quad \beta_{nkl..}^{(r)} = \frac{1}{r!} \frac{\partial^r D_n}{\partial x_k \partial x_l \dots} \bigg|_{\mathbf{x}=\bar{\mathbf{x}}}. \quad (11)$$

It can be shown that the coefficients $\alpha_{nkl..}^{(r)}$ and $\beta_{nkl..}^{(r)}$ are proportional to $(\beta \kappa \ell^2)^r$ (see Appendix A), and therefore, if κ is sufficiently small, higher order terms may be neglected in the expansion in eq.9. For $\ell = 8\text{nm}$, this requires $\kappa \ll 0.06\text{pN/nm}$, far smaller than the estimated value for kinesin (0.3pN/nm) [13, 14]. Nonetheless, for the sake of making further analytic progress, we proceed with this “weak coupling” approximation. When the expansion in eq.9 is thus truncated at $r = 1$, we obtain the LFPE

$$\begin{aligned} \frac{\partial \Pi}{\partial t} &\simeq \sum_{n=0}^N \frac{\partial}{\partial \eta_n} \left[\left(\dot{\bar{x}}_n - \bar{V}_n - \sum_k \alpha_{nk}^{(1)} \eta_k \right) \Pi \right] \\ &\quad + \frac{1}{2} \sum_{n=0}^N \bar{D}_n \frac{\partial^2 \Pi}{\partial \eta_n^2}. \end{aligned} \quad (12)$$

The averages and the correlation functions of η_n are defined as follows:

$$\langle \eta_p \rangle = \int \eta_p \Pi d\boldsymbol{\eta} \quad ; \quad \langle \eta_p \eta_q \rangle = \int \eta_p \eta_q \Pi d\boldsymbol{\eta}. \quad (13)$$

In order to satisfy the condition $\langle \eta_p \rangle = 0$, we put the convective term (corresponding to first order derivative with respect to η_n) in eq.12 to zero (see Appendix B), thereby arriving at the “macroscopic equations” [32]:

$$\dot{\bar{x}}_n = \bar{V}_n \quad ; \quad (0 \leq n \leq N). \quad (14)$$

By using the definition of $\langle \eta_p \eta_q \rangle$ given in eq.13, we obtain the dynamics of the correlation $\langle \eta_p \eta_q \rangle$ from eq.12 as follows (see Appendix B for the derivation):

$$\frac{d\langle \eta_p \eta_q \rangle}{dt} = \sum_{n=0}^N \left[\bar{D}_n \delta_{pn} \delta_{qn} + \alpha_{pn}^{(1)} \langle \eta_q \eta_n \rangle + \alpha_{qn}^{(1)} \langle \eta_p \eta_n \rangle \right]. \quad (15)$$

The results obtained in eqs.14 and 15 are very general and valid for arbitrary number of motors of either directionality.

2.2 Energy-dependence of motor hopping rates

We will now make specific choices for the functional form of motor hopping rates in the model. Let $E(\mathbf{x}) = (\ell^2/2) \sum_n \kappa_n \Delta_n^2$ be the total energy of the system in a configuration $\mathbf{x} \equiv \{x_0, x_1, \dots, x_N\}$. We define the local energy differences

$$\varepsilon_n^\pm = \pm [E(\dots x_n \pm 1, \dots) - E(\dots x_n, \dots)] = \frac{\kappa_n \ell^2}{2} [2\Delta_n \pm 1] \quad (16)$$

for a certain motor n at position x_n , corresponding to a single hop to its right or left. Then, we propose that the energy-dependent forward and backward hopping rates introduced earlier follow a local detailed balance condition, i.e.,

$$\frac{W_n^+(\Delta_n)}{W_n^-(\Delta_n + 1)} = \frac{w_n}{v_n} \exp(-\beta \varepsilon_n^+). \quad (17)$$

where $\beta = (k_B T)^{-1}$. The dynamic quantities that characterise the transport process, e.g. the instantaneous velocity of the motor and its diffusion coefficient depend on the difference and sum of the forward and backward rates respectively (eq.7). Hence, our results for these quantities will depend on the specific forms for the forward and backward rates satisfying eq.17. We consider a set of rates of the following form:

$$\begin{aligned} W_n^+(\Delta_n) &= w_n \exp[-\beta \varepsilon_n^+ \theta_n] \\ W_n^-(\Delta_n) &= v_n \exp[\beta \varepsilon_n^-(1 - \theta_n)] \end{aligned} \quad (18)$$

with $0 \leq \theta_n \leq 1$. This model has been studied extensively in the literature [28, 33, 34, 35, 36]. In some of these studies [33, 34], in the exponent, θ_n is accompanied by the external force exerted on the motor, whereas in our model (also in [35, 36]) it is accompanied by the energy difference ε_\pm . It is suggested in [34] that, θ_n determines the location of the transition state in the periodic free-energy landscape in which the motor takes steps.

In the next section, we will extract analytical expressions for several quantities of interest for a cargo driven by a set of identical motors ($w_n = w, v_n = v, \kappa_n = \kappa, \theta_n = \theta$) using the formalism developed so far. When motors are identical, the mean separation between motor and the

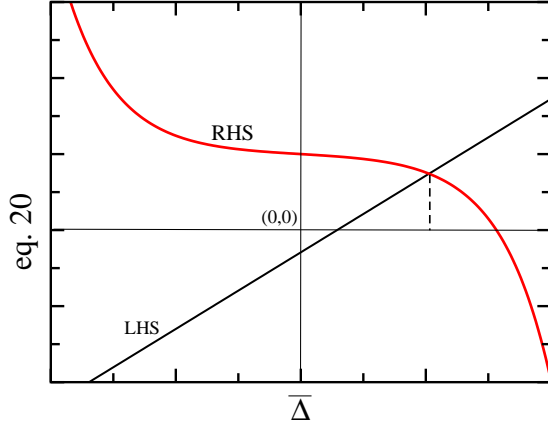


Fig. 3. The functions on left hand side (LHS) and right hand side (RHS) of the eq.20 are shown in this figure schematically. The solution to eq.20 is the value of $\bar{\Delta}$ at which LHS cuts the RHS in the figure (dashed line).

cargo, $\bar{\Delta} \equiv \bar{\Delta}_n$, is the same for all the motors. Also, $\bar{V}_n = \bar{V}_1$ and $\bar{D}_n = \bar{D}_1 \forall n \geq 2$. Further, the rates in eq.18 depends only on the separation $\Delta_n = x_n - x_0$, therefore by the definition of Taylor coefficients in eq.11, $\alpha_{n0}^{(1)} = -\alpha_{nn}^{(1)} \equiv \alpha$ for all $n \geq 1$. However $\alpha_{nm}^{(1)} = 0$ if $n, m \geq 1$ and $n \neq m$. Finally, $\alpha_{00}^{(1)} = -N\alpha_{0n}^{(1)} = -N\frac{\kappa}{\gamma}$. We use these quantities in the next section to analytically determine different properties characterising the dynamics of the motor-cargo complex.

2.3 Results for a cargo driven by identical motor proteins

(i) *Average cargo velocity:* For identical motors, since the hopping rates and stiffness of all the motors are equal, the mean separation between motor and the cargo is the same for all motors: $\bar{\Delta} \equiv \bar{\Delta}_n$. Therefore, from eqs.1, 8 and 10, the average cargo velocity is given by

$$V_{\text{avr}} \equiv \ell \bar{V}_0 = \frac{N\kappa\ell}{\gamma} \bar{\Delta} + \frac{f}{\gamma}, \quad (19)$$

In the steady state, both motors and cargo move essentially with the same velocity and therefore $\bar{V}_n = \bar{V}_0 \forall n \geq 1$. Hence, from eqs.7, 8 and 10, we arrive at the following transcendental equation for $\bar{\Delta}$:

$$\frac{N\kappa\ell}{\gamma} \bar{\Delta} + \frac{f}{\gamma} = \ell [W^+(\bar{\Delta}) - W^-(\bar{\Delta})] \quad (20)$$

Solution to eq.20 is to be reinserted in eq.19 to find the average cargo velocity.

Let us first understand the nature of solution to the transcendental eq.20 for the simple case where the external force on the cargo is zero ($f = 0$). The left hand side is a straight line with slope equal to $N\kappa\ell/\gamma$ passing through the origin. The right hand side is, in general, a smooth monotonic function of $\bar{\Delta}$ which varies from ∞

to $-\infty$ (see fig.3 for a schematic picture). Therefore, as the slope $N\kappa\ell/\gamma$ becomes larger and larger, the solution to the equation $\bar{\Delta}$ becomes smaller in magnitude (sign is positive if $w > v$ and negative if $w < v$). It suggests three different roles of κ, γ and N respectively in the transport mechanism: (a) When γ becomes larger, cargo experiences a large drag force while motors try to pull it away. This increases the motor-cargo separation as γ increases. (b) As κ is increased, the energy cost due to stretching increases, larger separation between motor and cargo is energetically unfavourable and this will enhance the backward hopping rate of the motor. As a result, we see a reduction in mean stretch $\bar{\Delta}$ with increase in κ . (c) Because all the motors are of same directionality, the number of springs which are connected in parallel increases (on an average) as N is increased. Due to additive nature of the spring constant in parallel springs, stretching of motors results in large energy cost and hence the mean separation between motor and cargo decreases with N . We will refer to these points again in subsequent sections where we use the specific rates given in eq.18 explicitly.

In the presence of external force ($f \neq 0$), the solution to the transcendental eq.20 depends on the directionality of the motor bound to the cargo. If the net motion of the cargo is towards plus direction (i.e. $w > v$) on the microtubule, then $f < 0$ corresponds to a resisting force and decrease in f would increase the magnitude of $\bar{\Delta}$. On the other hand if the net motion of the cargo is towards minus direction (i.e. $w < v$), then $f < 0$ corresponds to assisting force and decrease in f would decrease the magnitude of $\bar{\Delta}$.

(ii) *Effective diffusion coefficient:* Starting from eq.15, the long time behaviour of the variance $\langle \eta_i^2 \rangle$ can be calculated exactly for simple cases like $N = 1, 2$, results for which are given in Appendix B. Based on these results, we conjecture that for a cargo pulled by N motor proteins, the effective diffusion coefficient is

$$D_{\text{eff}}(N) = \ell^2 \left[\frac{\alpha^2 D_0 + N(\frac{\kappa}{\gamma})^2 \bar{D}_1}{2 \left(\alpha + N\frac{\kappa}{\gamma} \right)^2} \right]. \quad (21)$$

Interestingly, eq.21 implies that $D_{\text{eff}} \propto N^{-1}$ as $N \rightarrow \infty$.

N-dependence of V_{avr} and D_{eff} : The asymptotic result obtained above may be understood using an intuitive argument in the following way. For a free motor on the filament, w and v are forward and backward hopping rates respectively, with a fixed jump length ℓ . The average velocity and diffusion coefficient for this are given by $V_f = \ell(w - v)$ and $D_f = \ell^2(w + v)/2$ respectively. However, when multiple motor proteins are coupled through cargo, one may naively visualise whole system of motors as an effectual random walker pulling a cargo with modified hopping rates $w_e \sim Nw$, $v_e \sim Nv$ and jump length $\ell_e \sim \ell/N$. Then, the effective velocity $V_e = \ell_e(w_e - v_e)$ becomes independent of N while the effective diffusion coefficient $D_e = \ell_e^2(w_e + v_e)/2 \sim N^{-1}$ as $N \rightarrow \infty$. The scaling holds for a large range of stiffness, particularly when N is large. However, as discussed already, the exact effective

velocity and diffusion coefficient depend on the effective stiffness ($\kappa_e = N\kappa$) in a highly non-linear manner. This gives an additional weak N dependence to V_{avr} and D_{eff} at small N .

(iii) *Average force on the motor and force-fluctuations:*

The instantaneous force f_n on the n 'th motor is determined by the separation between the motor and cargo at that instant, i.e., $f_n = -\kappa\ell(x_n - x_0) = -\kappa\ell\Delta_n$. Because motor-cargo separation Δ_n changes randomly with time, f_n is also varies stochastically. The present formalism allows us to systematically determine the statistics of force experienced by the motor proteins and its load sharing properties. By the transformation of variables given in eq.3, we write the average force experienced by the motor as $\langle f_n \rangle = -\kappa\ell\bar{\Delta}$ for identical motors. $\langle f_n \rangle$ has two contributions: one is due to the external force f and other is due to the viscous drag force. To quantify the contribution by the viscous drag, we evaluated the difference between force experienced by the motor from f/N , i.e., define $\delta f = f_n - (f/N)$. From eq.19, we notice a relation between the average deviation in the force $\langle \delta f \rangle$ and the average cargo velocity V_{avr} , i.e.,

$$\langle \delta f \rangle = -\gamma \frac{V_{\text{avr}}}{N}, \quad (22)$$

which suggests that the contribution due to the viscous drag is negligible ($\langle f_n \rangle = f/N$) when $V_{\text{avr}} = 0$ i.e. when cargo is stalled or when the motors are large in number ($N \gg 1$).

It must be noted that equal [15] and stochastic [19,20] load-sharing models of motor-driven transport have been discussed in the literature. However, a meticulous study of force experienced by the motor and its deviation from mean field limit in stochastic load sharing model is still missing. The present formalism allows us to systematically determine the statistics of force experienced by the motor proteins and its load sharing properties. To investigate the deviation of force experienced by the motor from the mean field approximation, we study the standard deviation in the force experienced by the motor defined as $\sigma_f(N) = \sqrt{\langle f_n^2 \rangle - \langle f_n \rangle^2}$. In particular, note that if the force per motor is always the same, $\sigma_f(N)$ would vanish: this limiting behaviour is achieved when stiffness κ is sufficiently small, that is when motor-cargo interaction is negligible. With increase in the stiffness, fluctuations in the instantaneous force f_n relative to its mean value increases. As a result, $\sigma_f(N)$ is an increasing function of κ . It may be easily shown that $\sigma_f^2 = \kappa^2\ell^2[\langle \eta_n^2 \rangle + \langle \eta_0^2 \rangle - 2\langle \eta_0\eta_n \rangle]$ for $n \geq 1$. From the expressions for $\langle \eta_p\eta_q \rangle$ in Appendix B, specific results for $N = 1$ and $N = 2$ are obtained:

$$\begin{aligned} \sigma_f(1) &= \kappa\ell \sqrt{\left[\frac{D_0 + \bar{D}_1}{2\left(\alpha + \frac{\kappa}{\gamma}\right)} \right]}, \\ \sigma_f(2) &= \kappa\ell \sqrt{\left[\frac{\alpha D_0 + (\alpha + \frac{\kappa}{\gamma})\bar{D}_1}{2\alpha(\alpha + 2\frac{\kappa}{\gamma})} \right]}. \end{aligned} \quad (23)$$

Because \bar{D}_1 is a function of κ , the nature of the dependence of σ_f on κ is not obvious from eq.23. However, as we will see later from numerical simulation that, $\sigma_f(N)$ is an increasing function of κ and N .

(iv) *Stall force:* To determine the expression for stall force f_s^N (force corresponding to vanishing cargo velocity, i.e., $V_{\text{avr}} = 0$) within this formalism, we put the RHS of eq.20 to zero, the solution of which may be denoted $\Delta_s(\kappa)$. Then, from the LHS, the stall force is given by $f_s(\kappa) = -N\kappa\ell\Delta_s(\kappa)$: after substitution of $\Delta_s(\kappa)$ we find the stall force to be

$$f_s^N = N \left[\frac{1}{\beta\ell} \log\left(\frac{v}{w}\right) - \kappa\ell\left(\frac{1}{2} - \theta\right) \right] \quad (24)$$

Eq.24 completes the set of results we obtained from our approximate analytical treatment of the problem. We now proceed to discuss the results from numerical simulations.

2.4 Numerical simulations

In numerical simulations, we used Brownian dynamics for cargo motion, along with fixed time-step kinetic Monte-Carlo scheme for motor dynamics. All the motors and the cargo are initialised at $x_n = 0$ ($0 \leq n \leq N$) at $t = 0$ and their locations are updated in each time step $\delta t = 10^{-5}s$. From the noted locations of the cargo and all the motors ($x_0, x_1 \dots x_N$) in the present time t , the separation between n 'th motor and the cargo $\Delta_n = x_n - x_0$ is used to determine the force on the cargo $f_c = \kappa\ell \sum_{n=1}^N \Delta_n$ and the energy cost for forward/backward jump $\varepsilon_n^\pm = (\kappa_n\ell^2/2)[2\Delta_n \pm 1]$. In the next time step $t + \delta t$, the location of the cargo is estimated according to the over-damped Langevin equation (eq.1) and motor locations are updated using the rates given in eq.18. Position of the cargo and all the individual motors are recorded for a long time (this time scale depends on the number of motors N and stiffness κ ; the time required to reach steady state is different in each cases, but typically varies from 5s to 25s), which enabled us to determine various averaged quantities of interest in the steady state. In particular, the average velocity is estimated from the relation $\langle \delta x \rangle / \delta \tau$ where, $\langle \delta x \rangle$ is the average distance covered in the observation time $\delta \tau$. The averaging is carried out over several identical copies (typically 50000) of the system. Similarly the effective diffusion coefficient is evaluated as $[\langle \delta x^2 \rangle - \langle \delta x \rangle^2] / 2\delta \tau$.

2.5 Comparing theory and simulations

Velocity versus κ : We have chosen the set of parameters given in Table 1, and found the solution for $\bar{\Delta}$ from the transcendental equation 20 numerically. Then the average cargo velocity V_{avr} is evaluated from eq.19. As explained earlier, due to increase in energy cost for the movement of motors on the filament, average separation $\bar{\Delta}$ is reduced at larger κ . Therefore, the average velocity of the cargo decreases with κ . Increase in the number of motors results

β pN ⁻¹ nm ⁻¹	γ pNs nm ⁻¹	w s ⁻¹	v s ⁻¹	ℓ nm	θ
0.2433	9.42×10^{-4}	125.0028	0.0028	8	0.1

Table 1. A list of parameters used in our calculations and numerical simulations are shown here. The value for γ is chosen from [22]. For kinesin, $\ell = 8\text{nm}$ is observed [37] and $\theta = 0.1$ is the typical value used for the same motor in [24]. Rates w and v are chosen in such a way that the free motor velocity $V_f = \ell(w - v)$ and the stall force of the free motor $f_s^1 = \ln(v/w)/(\beta\ell)$ are equal to $1\mu\text{ms}^{-1}$ and -5.5pN respectively.

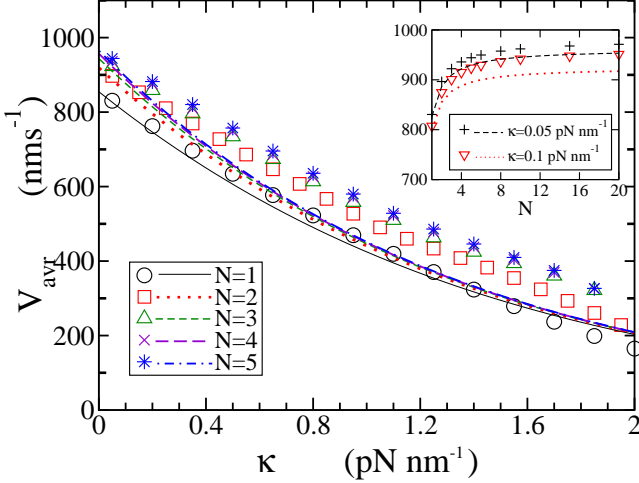


Fig. 4. Average cargo velocity V_{avr} is shown as a function of stiffness at zero external force ($f = 0$), for various numbers of cargo-bound motors. In inset, V_{avr} is shown as a function of number of motors N , at two different values of the stiffness. The dashed line is the analytical result obtained from eq.19 and the symbols are computer simulation results.

in a very small increase in the velocity at small κ , but the enhancement is negligibly small at large κ and large N . We can see these effects in fig.4 where analytical results (lines) show good agreement with simulations (symbols).

Diffusion coefficient versus κ : Because both forward and backward hopping rates decrease with increase in κ , the overall movement itself is hindered. Fluctuations about the mean are suppressed by the increase in stretching energy cost at large stiffness. Therefore, the effective diffusion coefficient D_{eff} (see eq.21) of the motor-cargo assembly, as predicted by theory, decreases with κ and vanishes asymptotically. Results for D_{eff} as a function of κ are shown in fig.5(a). Simulation results [symbols in fig.5(a)] also show good agreement with these observations. We see in fig.5(b) that, D_{eff} decreases with N and the dependence becomes proportional to $1/N$ asymptotically, which is confirmed by the slope in the inset. We have seen in fig.4 that the velocity remains constant at larger motor numbers although it increases initially with N . Therefore, as N increases, multiple motor-mediated transport becomes more deterministic.

Mean force experienced by a motor and its load sharing features: In fig.6, the average force experienced by each motor $\langle f_n \rangle = -\kappa\ell\Delta_n$ is shown as a function of κ . Even

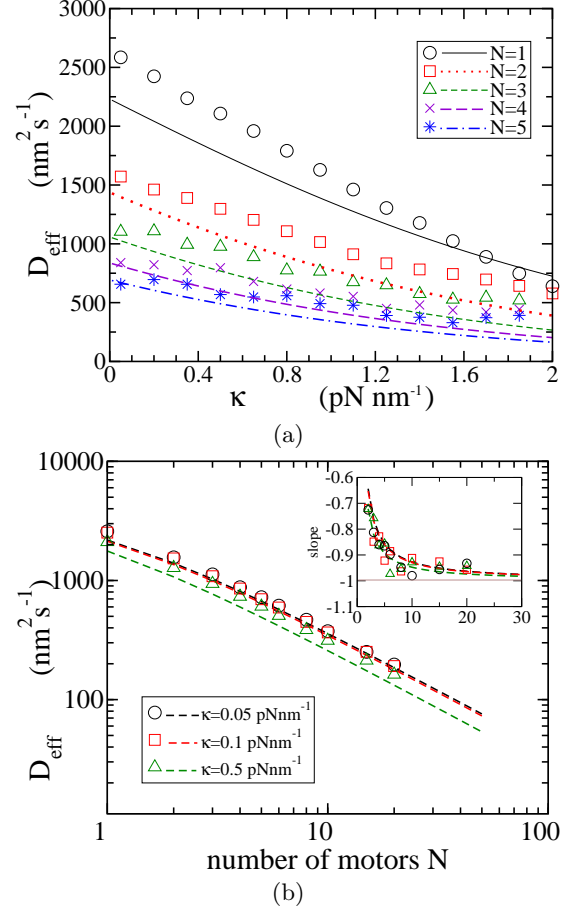


Fig. 5. The effective diffusion coefficient (D_{eff}) of the cargo as a function of stiffness is shown in (a) for various numbers of cargo-bound motors. D_{eff} decreases with stiffness as well as number of motors on the cargo. In (b), D_{eff} is shown on a logarithmic scale against number of motors in for three different κ . The slope of this line, equal to $[\ln D_{\text{eff}}(N+1) - \ln D_{\text{eff}}(N)]/[\ln(N+1) - \ln(N)]$, approaches -1 as N increases, indicating that D_{eff} decreases as $1/N$ asymptotically (see inset). In both (a) and (b), dashed lines correspond to eq.21 and symbols are simulation results.

in the absence of external load on the cargo ($f = 0$), due to the competition between viscous drag and elastic stretching, a motor experiences a net opposing force, whose average is $\langle f_n \rangle = -\gamma V_{\text{avr}}/N$. The decrease of $\langle f_n \rangle$ as a function of κ is related to the reduction in V_{avr} with increasing stiffness. With increase in number of motors N , V_{avr} becomes independent of N (see fig.4 insets) and therefore, the force experienced by each motor decreases as $1/N$ asymptotically.

We have looked at the dependence of $\langle \delta f \rangle$ (the average force on the motor due to viscous drag) on the stiffness, in the presence of external force $f = -3\text{pN}$. The analytical expression (eq.22), in comparison with simulation results, is shown in fig.7 insets. Notably, the average force on the motor due to viscous drag in the absence of external force, shown in fig.6, is slightly larger than that in the presence of force $f = -3\text{pN}$, as shown in fig.6 insets.

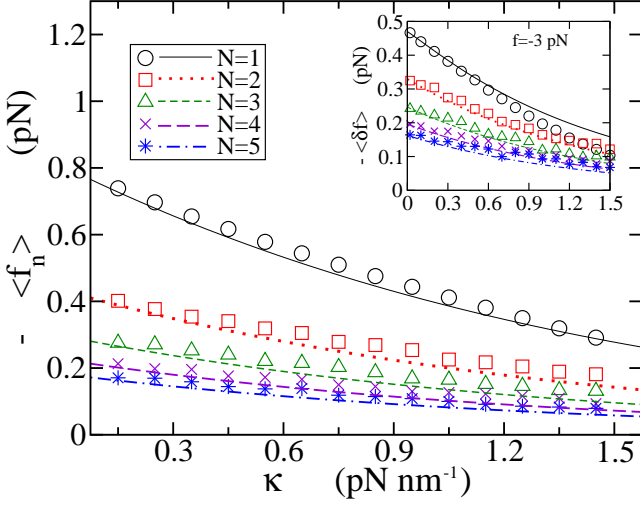


Fig. 6. The figure shows the mean force experienced by each motor $\langle f_n \rangle = -\kappa \ell \bar{\Delta}$ as a function of stiffness at $f = 0$. Inset shows the force experienced by the motor due to the viscous drag in the medium $\langle \delta f \rangle = \langle f_n \rangle - (f/N)$ at force $f = -3$ pN. Symbols correspond to results obtained in computer simulations.

This is expected because the opposing force reduces the average velocity of the motor-cargo complex, thereby reducing the viscous drag force on it. Further, with increase in stiffness, the average velocity of the motor decreases, and hence the force experienced due to the drag force also reduces accordingly.

The mean squared fluctuation $\sigma_f(N)$ which quantifies the load sharing properties is shown in fig.7 for $N = 1$ and 2. From both simulations (symbols) as well as the analytical expression (eq.23, lines), we see that $\sigma_f(N)$ is an increasing function of κ , i.e., when motors are weakly interacting, they share load equally. For typical κ and N , the deviation is not small- almost 1 pN for $N = 1$ and 2 pN for $N = 2$, when $\kappa = 0.5$ pN nm⁻¹; the numbers become 2.5 pN for $N = 1$ and 4 pN for $N = 2$ when the stiffness is 1.5 pN nm⁻¹. The inset of fig.7 shows the coefficient of variation $r = \sigma_f(N)/\langle f_n \rangle$ for $N = 1, 2$. Note that while r is less than (but comparable to) 1 for $N = 1$ (for $\kappa < 1.5$ pN/nm), it is typically greater than one for $N = 2$. Force experienced by an individual motor in an assembly is subject to large relative fluctuations when N is large.

The average force experienced by the motor in the presence of elastic motor-cargo coupling has been studied numerically by Kunwar et al.[20] and it has been shown that, the force experienced by the motor decreases with the stiffness, similar to what we have seen in fig.6. Moreover, in their work, broadening of the distribution of force experienced by the motor with increases in the stiffness was also observed, which is captured by $\sigma_f(N)$ in fig.7 in our study.

Velocity versus f : We studied the force-velocity curve for a cargo driven by a single motor ($N = 1$) at various stiffnesses, results of which are shown in fig.8. We see that, for the chosen set of parameters in Table 1, the force-velocity curve is convex-up. The comparison with com-

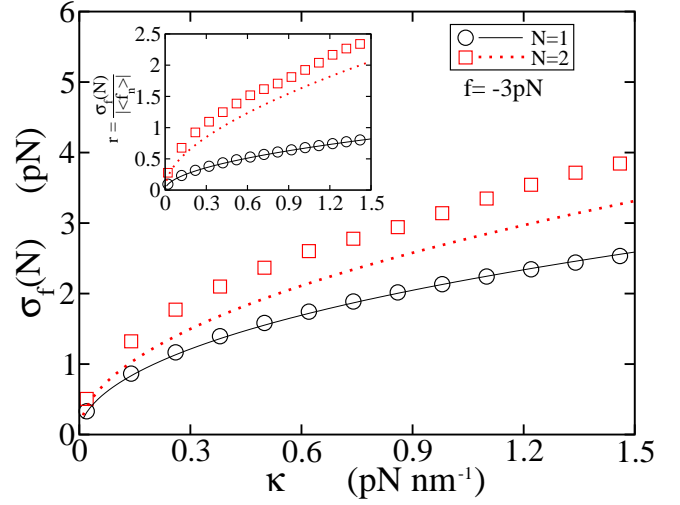


Fig. 7. The standard deviation $\sigma_f(N)$ (eq.23) of force experienced by a single motor is shown here as a function of stiffness at $f = -3$ pN. Inset shows, the fluctuation to mean ratio $r = \sigma_f(N)/\langle f_n \rangle$ at $f = -3$ pN. The symbols are results obtained in computer simulations while the line corresponds to analytical result.

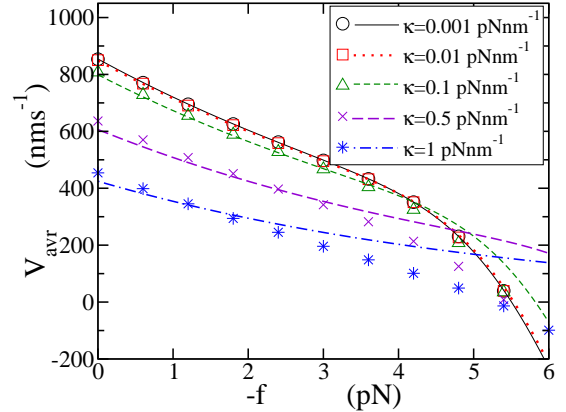


Fig. 8. The force-velocity curve is shown for a cargo driven by a motor protein ($N = 1$) at different stiffnesses κ of the motor-cargo linker (dashed line, eq.19). The computer simulation results are shown as symbols.

puter simulations (symbols) show nice agreement with the theoretical results at small opposing forces ($f < 0$), while significant deviation is observed at larger opposing forces, particularly close to the regime where velocity becomes zero. Interestingly, in simulations, the velocity appears to cross zero at the same force for all κ values, indicating that the stall-force is independent of κ ; a more detailed discussion on the same is given in the next paragraph.

Stall force versus κ : We looked at stall-force $f_s^N(\kappa)$ as a function of κ for a cargo driven by varying numbers of motor proteins. For fast convergence in simulations, we replaced the constant force f with a harmonic trap force $f = -\kappa_t x$ where κ_t is the trap stiffness, whose value was chosen as 0.5 pN nm⁻¹ (we have performed some simulations in the constant force ensemble also, and verified that the results are not affected). The results for stall force as a

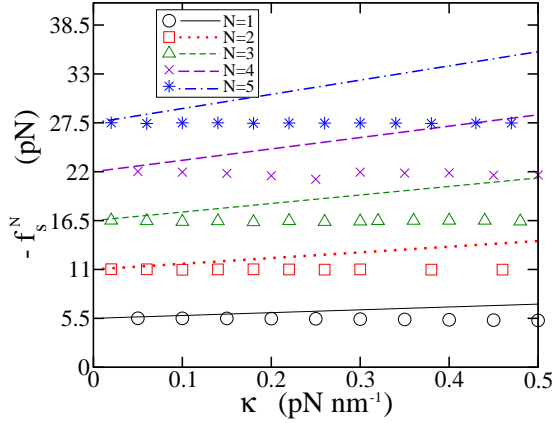


Fig. 9. The results for stall force as a function of stiffness κ is shown here for different N . The computer simulation results are shown as symbols. The dashed line corresponds to the analytical expression given in eq.24.

function of stiffness is shown in fig.9 for different numbers of cargo bound motors. In numerical simulations (symbols in the figure), the stall force is found to be independent of κ . However, the expression for the stall force given in eq.24 disagrees with simulations, except in the limit $\kappa \rightarrow 0$. The underlying reason is presumably the neglect of higher order terms in the expansion of the master equation (eq.12), not captured in the first order perturbation approximation. To justify this argument, in Appendix A, we have given the Taylor coefficients (eq.11) of different orders in the presence of the stall force of the motor proteins and show that higher order terms are not negligible when κ is large.

It is also pertinent to point out that force-velocity behaviour of two elastically coupled motor proteins has been studied in [27], where stall force is found to be dependent on the stiffness. However, there are two key differences between our model and that in [27]. (i) In [27], forward hopping rate of the individual motor is linearly dependent on the force (which is derived from linear force-velocity relation), while backward hopping is absent. In our model, more general, thermodynamically consistent rates (eq.18) are used. (ii) Detachment of motors from the filament with load-dependent detachment rates is included in [27], while it is ignored in our study. We are presently developing an extended version of our model, which also includes motor detachment from the filament.

3 Comparison with experiments

In order to check how well our model describes the observed features of real motors, we study the force-velocity behaviour of kinesins reported in [37]. In the experiment, the velocity of a motor protein attached to a silica bead was studied by exerting controlled loads using an optical trap, in the presence of different ATP concentrations. The force-velocity behaviour found in Visscher et al. (1999) at $5\mu\text{M}$ and 2mM ATP concentration is displayed as squares in fig.10(a) and (b) respectively. We managed to reproduce

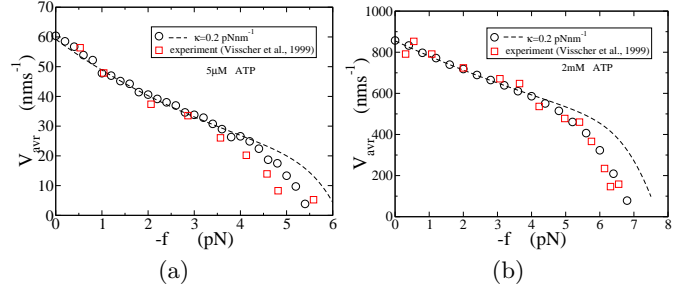


Fig. 10. In (a) and (b), the force-velocity behaviour predicted from our theory and simulation is compared with the force-velocity behaviour of kinesin observed by Visscher et al. [37] at $5\mu\text{M}$ and 2mM ATP concentrations respectively. In both (a) and (b), experimental data (used with the permission of the publishers) are given as squares, analytical results as dashed lines and numerical simulations in circles.

these results by tuning a few parameters in our model. The values of ℓ , β and γ are same as that in Table 1. The forward and backward hopping rates of the motor (w and v) are determined in such a way that the single free motor velocity [$V_f = \ell(w - v)$] and stall force [$f_s^1 = \ln(v/w)/\beta\ell$] are consistent with experimental observations in [37]. Specifically, at $5\mu\text{M}$ ATP concentrations, velocity and stall force of the motor are close to 70nm s^{-1} and -5.5pN respectively, from which we get $w \approx 8.745\text{s}^{-1}$ and $v \approx 1.96 \times 10^{-4}\text{s}^{-1}$. Similarly, at 2mM ATP concentration velocity and stall force are respectively 1000nm s^{-1} and -7pN , using which we get $w \approx 125\text{s}^{-1}$ and $v \approx 1.52 \times 10^{-4}\text{s}^{-1}$. The value of θ is reduced slightly (from 0.1 to 0.05) in order to get more accurate behaviour for 2mM ATP concentration case. The force-velocity behaviour obtained mathematically (dashed line) and computationally (circles) at stiffness $\kappa = 0.2\text{pN nm}^{-1}$ is shown in fig.10(a) and (b) at $5\mu\text{M}$ and 2mM ATP concentrations respectively. However, at larger values of κ , the results do not seem to show good agreement with experimental observations. Further, as the external force on the motor approaches the stall force, analytical results show a slight deviation from computer simulation results, suggesting the relevance of higher order corrections.

4 Summary and Conclusions

In this paper, we explored the effects of elastic coupling between a cargo and the attached molecular motors on the statistical properties of transport. In our model, we regarded motor domains of these proteins as biased random walkers with fixed jump length, while the cargo is subjected to thermal noise and an external applied force, in addition to elastic forces from the motors. To capture the elastic energy dependence of motor hopping rates, asymmetric exponential forms given in eq.18 were used. The stochastic hopping dynamics for N motor proteins, along with the over-damped Langevin equation for cargo motion (eq.1) leads to a $(N + 1)$ -variable composite master equation for the dynamics of the motor-cargo assembly.

Employing a transformation of variables and first order perturbation expansion in the master equation governing the motor-cargo dynamics, the dynamics of the average quantities was systematically separated from that of fluctuations. The former satisfies a set of deterministic “macroscopic” equations, while the latter are governed by a LFPE, which yields equations for the various moments and correlation functions. Both sets of equations were solved numerically to determine quantities of interest such as the average velocity and mean force experienced by the motor, effective diffusion coefficient of the motor-cargo complex and information on load sharing between the motors. Using our model, we also reproduced the force-velocity behaviour of kinesin observed in an experiment [37] by minimal tuning of parameters.

We made the following important observations in course of our study. (i) The average velocity and the effective diffusion coefficient of the motor cargo assembly reduces with increase of the elastic coupling constant κ . Our results are consistent with some of the observations made in earlier studies [25,26] where it was reported that, the average cargo velocity reduces as a function of stiffness of the motor-cargo linker. (ii) Asymptotically, the average velocity becomes independent of motor number N while the effective diffusion constant decreases as $1/N$. (iii) Even in the absence of external force, all the motors experience a load due to viscous drag of the cytoplasm. The average force experienced by a motor decreases with κ , and this observation is consistent with earlier study by Kunwar et al.[20]. In the presence of opposing external force on the cargo, the average velocity of the cargo decreases and hence the force due to the viscous drag also reduces accordingly. (iv) When κ is very small, motors are almost non-interacting and the force on the cargo is shared equally among the motors. On the other hand, as κ becomes larger, the deviation from this “mean field” behaviour becomes significant. Kunwar et al.[20] too have reported large fluctuations in the force experienced by individual motor in a team of two motors pulling a cargo. (iv) The stall force is found to be independent of the stiffness κ in simulations, but this behaviour is not captured by the analytical results due to the neglect of relevant higher order terms in the Kramers-Moyal expansion.

The complete absence of κ -dependence in the stall force is an important observation in our study, something which our analytical treatment failed to reproduce. This has important implications; for instance, this result guarantees that the stall force measured for a motor using a glass bead as cargo in an in vitro optical trap experiment may be expected to be valid for a more flexible intracellular cargo also. Recent experiments on transport of DNA-scaffold by motors having controlled separation between them, have opened possibility of studying directly motor-motor interaction between like motors during transport [12]. In such experiments, it may be possible to verify some of our predictions. We hope that the formalism developed here and its possible future extensions will be found useful in quantitative modelling of cargo transport involving multiple motor proteins.

The authors would like to thank P.G. Senapathy Centre for Computing Resources, IIT Madras for computational support. DB thanks Udo Seifert for stimulating discussions during the Non-equilibrium Statistical Physics Workshop (2015) held at ICTS, Bengaluru. DB also acknowledges Sumesh Thampi, Raghunath Chelakkot and Amitabha Nandi for useful conversations.

A On the relevance of higher order terms in the Kramers-Moyal expansion

The Taylor coefficients $\alpha_{nkl\dots}^{(r)}$ and $\beta_{nkl\dots}^{(r)}$ given in eq.11 are derivatives of V_n and D_n respectively, evaluated at $\mathbf{x} = \bar{\mathbf{x}}$. As we see from eq.8, V_0 is function of all the variables $(x_0, x_1 \dots x_N)$, but depends only linearly on them. So corresponding coefficients of order larger than one in the Taylor expansion are zero identically, i.e. $\alpha_{0kl\dots}^{(r)} = 0$ for $r \geq 2$. $D_0 = D/\ell^2$ is a constant, so all $\beta_{0kl\dots}^{(r)}$ for $r \geq 1$ are zero. However, from eqs.7 and 18, we can see that the higher order coefficients in Taylor expansion of V_n and D_n are non-zero for $n \geq 1$. But, V_n and D_n are functions of only x_n and x_0 through $\Delta_n = x_n - x_0$. Therefore, those terms involving cross derivatives i.e. $\alpha_{nkl\dots}^{(r)}$ and $\beta_{nkl\dots}^{(r)}$ with $k, l, \dots \neq n$ and $k, l, \dots \neq 0$ are zero [only for $k, l, \dots = n, 0$, $\alpha_{nkl\dots}^{(r)}$ and $\beta_{nkl\dots}^{(r)}$ survive]. Further, the coefficients with $k = n$ corresponding to derivative with respect to x_n and those with $k = 0$ corresponding to derivative with respect to x_0 (keeping rest of the suffices same), differ only by sign. Therefore, it is enough to study the coefficients corresponding to $k = l = \dots = n$ i.e. $\alpha_{nnn\dots}^{(r)}$ and $\beta_{nnn\dots}^{(r)}$ for $n \geq 1$. From eqs.7, 11 and 18, these are given by

$$\alpha_{nnn\dots}^{(r)} = \frac{(\beta\kappa_n\ell^2)^r}{r!} [(-\theta_n)^r W_n^+(\bar{\Delta}_n) - (1 - \theta_n)^r W_n^-(\bar{\Delta}_n)],$$

$$\beta_{nnn\dots}^{(r)} = \frac{(\beta\kappa_n\ell^2)^r}{r!} [(-\theta_n)^r W_n^+(\bar{\Delta}_n) + (1 - \theta_n)^r W_n^-(\bar{\Delta}_n)] \quad (25)$$

Further, for identical motors, $\bar{\Delta}_n = \bar{\Delta}$, $\theta_n = \theta$, $w_n = w$, $v_n = v$ and therefore, at fixed N , $\alpha_{nnn\dots}^{(r)} = \alpha_{111\dots}^{(r)}$ and $\beta_{nnn\dots}^{(r)} = \beta_{111\dots}^{(r)}$ for all $N \geq n \geq 2$. In fig.11, Taylor coefficients $\alpha_{111\dots}^{(r)}$ and $\beta_{111\dots}^{(r)}$ shown (up to $r = 5$) for $N = 1$ at different κ and θ values. For the chosen set of parameters given in Table 1, when $\theta = 0.1$ the terms corresponding to $r = 1$ are predominant in the range of stiffness we considered in this study ($0 - 2pNm^{-1}$). Therefore, the formalism developed here shows overall agreement with computer simulations. On the other hand, at $\theta = 0.5$ and $\theta = 0.9$, higher order terms become important and so the formalism developed here is not appropriate at these θ values. But, at very small κ values such that $\beta\kappa\ell^2 \ll 1$, we see from eq.25 that the higher order Taylor coefficients are small, and so the formalism is valid in this regime.

In fig.12 and fig.13, we have shown results for V_{avr} and D_{eff} as a function of κ obtained in computer simulations at $\theta = 0.5$ and $\theta = 0.9$. The variation in the velocity and diffusion coefficient as a function of stiffness κ is qualitatively similar to that of $\theta = 0.1$. However, now a large deviation from the analytical results is seen, which highlights the inaccuracy of our approximation for these parameter values.

For the set of parameters in Table 1, the Taylor coefficients $\alpha_{111\dots}^{(r)}$ and $\beta_{111\dots}^{(r)}$ evaluated at $f = -5.5pN$ are also shown for $N = 1$ in the fig.14. We saw in fig.11 (for $\theta = 0.1$ column) that, when $f = 0$, only the first order coefficients are important within the range of stiffness considered. However at $f = -5.5pN$, all the

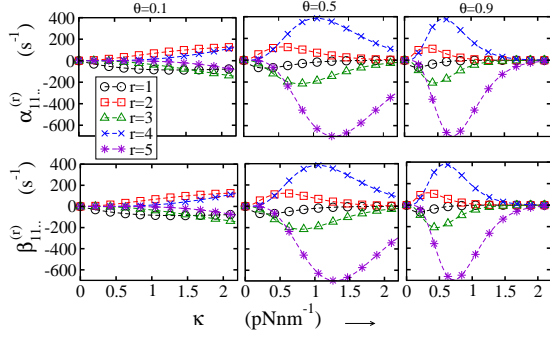


Fig. 11. Taylor coefficients $\alpha_{11..}^{(r)}$ and $\beta_{11..}^{(r)}$ given in eq.25 are shown here (up to $r = 5$) as function of κ at $\theta = 0.1$, $\theta = 0.5$ and $\theta = 0.9$. For $\theta = 0.1$ higher order terms are much smaller compare to first order terms. On the other hand for $\theta = 0.5$ and $\theta = 0.9$, higher order terms are significant.

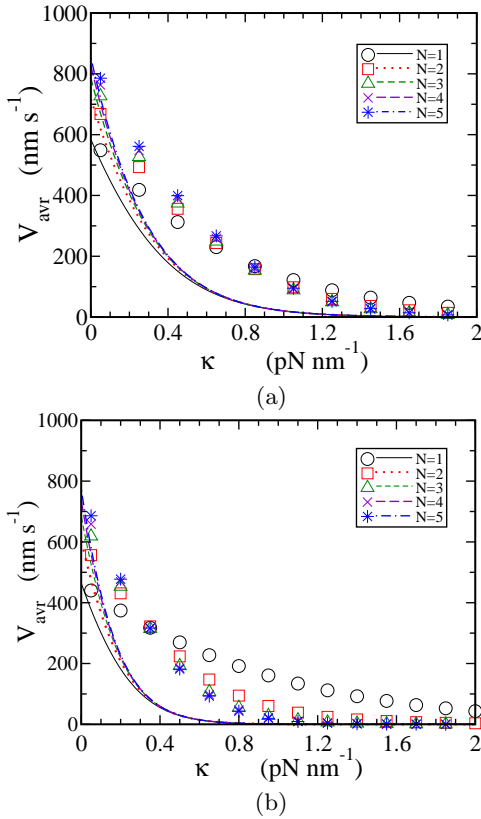


Fig. 12. Average velocity of the cargo as a function of stiffness is shown here for $\theta = 0.5$ in (a) and $\theta = 0.9$ in (b). All the other parameters are chosen from Table 1. The deviation of analytical results (lines) from simulation (symbols) is significant in these cases, compared to that in $\theta = 0.1$ case (fig.4).

higher order terms are large compared to first order terms. This results in the deviation of analytical results for stall force from the computer simulations in fig.9.

B Evaluation of effective diffusion coefficient

$\Pi(\eta)$ in eq.12 is function of fluctuations $\eta \equiv \{\eta_0, \eta_1, \dots, \eta_N\}$. We define the Fourier transform of Π with respect the variables η

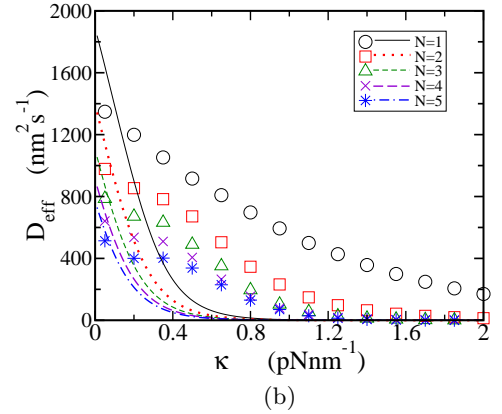
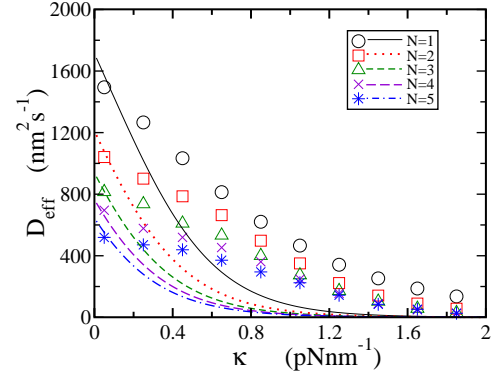


Fig. 13. Effective diffusion coefficient of the motor-cargo assembly is shown as a function of stiffness here for $\theta = 0.5$ in (a) and $\theta = 0.9$ in (b). Here, rest of the parameters are chosen from Table 1. The deviation of analytical results (lines) from simulation (symbols) is significant here due to prominent higher order corrections.

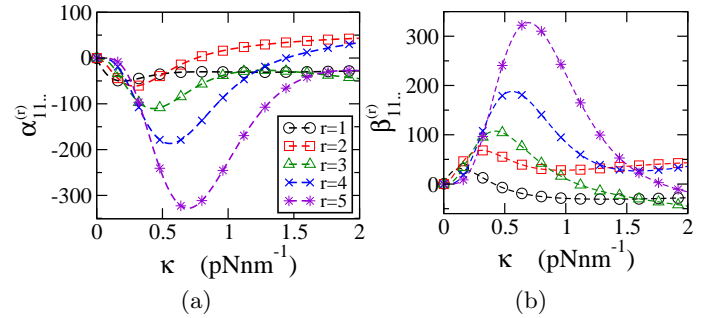


Fig. 14. The coefficients $\alpha_{11..}^{(r)}$ and $\beta_{11..}^{(r)}$ given in eq.25 are shown as function of κ at $f = -5.5\text{pN}$ for $N = 1$. Rest of the parameters are chose from Table 1.

as:

$$\mathcal{F}[\Pi(\eta)] \equiv \Phi(g) = \int \exp[ig \cdot \eta] \Pi(\eta) d\eta_0 d\eta_1 \dots$$

Using properties of the Fourier transform,

$$\mathcal{F} \left[\frac{\partial^m \Pi(\eta)}{\partial \eta_n^m} \right] = (-ig_n)^m \Phi(g) ; \quad \mathcal{F} [\eta_n \Pi(\eta)] = \frac{\partial \Phi(g)}{\partial (ig_n)}$$

eq.12 may be rewritten as follows:

$$\frac{\partial \Phi}{\partial t} = \sum_{n=0}^N (-ig_n) \left[(\dot{x}_n - \bar{V}_n) \Phi - \sum_k \alpha_{nk}^{(1)} \frac{\partial \Phi}{\partial (ig_k)} \right] - \frac{1}{2} \sum_{n=0}^N \bar{D}_n g_n^2 \Phi \quad (26)$$

Some useful properties of Φ here are:

$$\langle \eta_p \rangle = \frac{\partial \Phi}{\partial (ig_p)} \Big|_{g=0} \quad \text{and} \quad \langle \eta_p \eta_q \rangle = \frac{\partial^2 \Phi}{\partial (ig_p) \partial (ig_q)} \Big|_{g=0} \quad (27)$$

From eq.26 and the definition of $\langle \eta_p \rangle$ in eq.27, we arrive at:

$$\frac{d}{dt} \langle \eta_p \rangle = \sum_{n=0}^N \alpha_{pn}^{(1)} \langle \eta_n \rangle - (\dot{x}_p - \bar{V}_p) \quad (28)$$

As $\{\eta_p\}$ are defined as fluctuations about averages \bar{x}_p , we require that $\langle \eta_p \rangle = 0$, which is realized by putting the non-homogeneous term in eq.28 to zero, thereby arriving at eq.14.

Further, using the condition $\langle \eta_p \rangle = 0$, from eq.26 and the definition of $\langle \eta_p \eta_q \rangle$ in eq.27, we obtain:

$$\frac{d \langle \eta_p \eta_q \rangle}{dt} = \sum_{n=0}^N \left[\bar{D}_n \delta_{pn} \delta_{qn} + \alpha_{pn}^{(1)} \langle \eta_q \eta_n \rangle + \alpha_{qn}^{(1)} \langle \eta_p \eta_n \rangle \right]. \quad (29)$$

For $N = 1$, second moments and correlation functions are found explicitly as follows:

$$\begin{aligned} \frac{d}{dt} \langle \eta_0^2 \rangle &= D_0 + \frac{\kappa}{\gamma} [\langle \eta_0 \eta_1 \rangle - \langle \eta_0^2 \rangle] \\ \frac{d}{dt} \langle \eta_1^2 \rangle &= \bar{D}_1 + \alpha [\langle \eta_0 \eta_1 \rangle - \langle \eta_1^2 \rangle] \\ \frac{d}{dt} \langle \eta_0 \eta_1 \rangle &= \alpha \langle \eta_0^2 \rangle + \frac{\kappa}{\gamma} \langle \eta_1^2 \rangle - \left(\alpha + \frac{\kappa}{\gamma} \right) \langle \eta_0 \eta_1 \rangle \end{aligned} \quad (30)$$

To solve the above equations, we define the Laplace transforms $\langle \eta_p \eta_q \rangle_s = \int_0^\infty \exp(-st) \langle \eta_p \eta_q \rangle dt$. eq.30 is now expressed in matrix form and solved for the moments in Laplace space. For $N = 1$, the complete solution is

$$\begin{aligned} \langle \eta_0^2 \rangle_s &= \frac{[D_0 s^2 + D_0(3\alpha + \frac{\kappa}{\gamma})s + 2\alpha^2 D_0 + 2(\frac{\kappa}{\gamma})^2 \bar{D}_1]}{s^2(s + \alpha + \frac{\kappa}{\gamma})(s + 2\alpha + 2\frac{\kappa}{\gamma})} \\ \langle \eta_1^2 \rangle_s &= \frac{[\bar{D}_1 s^2 + \bar{D}_1(\alpha + 3\frac{\kappa}{\gamma})s + 2\alpha^2 D_0 + 2(\frac{\kappa}{\gamma})^2 \bar{D}_1]}{s^2(s + \alpha + \frac{\kappa}{\gamma})(s + 2\alpha + 2\frac{\kappa}{\gamma})} \\ \langle \eta_0 \eta_1 \rangle_s &= \frac{[(D_0 \alpha + \bar{D}_1 \frac{\kappa}{\gamma})s + 2\alpha^2 D_0 + 2(\frac{\kappa}{\gamma})^2 \bar{D}_1]}{s^2(s + \alpha + \frac{\kappa}{\gamma})(s + 2\alpha + 2\frac{\kappa}{\gamma})}. \end{aligned} \quad (31)$$

We observe that as $s \rightarrow 0$, $\langle \eta_0^2 \rangle_s = \langle \eta_1^2 \rangle_s \approx 2(D_{\text{eff}}/\ell^2 s^2)$, and hence $\langle \eta_0^2 \rangle = \langle \eta_1^2 \rangle \approx 2(D_{\text{eff}}/\ell^2)t$ where D_{eff} is the effective one-dimensional diffusion coefficient of the cargo on the filament, given by

$$D_{\text{eff}}(1) = \ell^2 \left[\frac{\alpha^2 D_0 + (\frac{\kappa}{\gamma})^2 \bar{D}_1}{2(\alpha + \frac{\kappa}{\gamma})^2} \right]. \quad (32)$$

For $N = 2$, a similar analysis gives the moment-transforms

$$\begin{aligned} \langle \eta_0^2 \rangle_s &= \frac{D_0 s^2 + D_0(3\alpha + 2\frac{\kappa}{\gamma})s + 2\alpha^2 D_0 + 4\bar{D}_1(\frac{\kappa}{\gamma})^2}{s^2(s + \alpha + 2\frac{\kappa}{\gamma})(s + 2\alpha + 4\frac{\kappa}{\gamma})} \\ \langle \eta_1^2 \rangle_s &= \langle \eta_2^2 \rangle_s = \frac{\bar{D}_1 s^3 + \frac{\bar{D}_1}{2}(2\frac{\kappa}{\gamma} + \alpha)s^2}{s^2(s + 2\alpha)(s + \alpha + 2\frac{\kappa}{\gamma})(s + 2\alpha + 4\frac{\kappa}{\gamma})} + \\ &\quad \frac{2[\alpha^2(D_0 + \bar{D}_1) + 4(\frac{\kappa}{\gamma})^2 \bar{D}_1 + 3\alpha(\frac{\kappa}{\gamma})\bar{D}_1]s + 4\alpha^3 D_0 + 8\alpha\bar{D}_1(\frac{\kappa}{\gamma})^2}{s^2(s + 2\alpha)(s + \alpha + 2\frac{\kappa}{\gamma})(s + 2\alpha + 4\frac{\kappa}{\gamma})} \\ \langle \eta_0 \eta_1 \rangle_s &= \langle \eta_0 \eta_2 \rangle_s = \frac{[(\alpha D_0 + \bar{D}_1 \frac{\kappa}{\gamma})s + 2\alpha^2 D_0 + 4(\frac{\kappa}{\gamma})^2 \bar{D}_1]}{s^2(s + \alpha + 2\frac{\kappa}{\gamma})(s + 2\alpha + 4\frac{\kappa}{\gamma})} \\ \langle \eta_1 \eta_2 \rangle_s &= \frac{2\alpha [(\alpha D_0 + \bar{D}_1 \frac{\kappa}{\gamma})s + 2\alpha^2 D_0 + 4(\frac{\kappa}{\gamma})^2 \bar{D}_1]}{s^2(s + 2\alpha)(s + \alpha + 2\frac{\kappa}{\gamma})(s + 2\alpha + 4\frac{\kappa}{\gamma})}. \end{aligned} \quad (33)$$

Similar to the previous case, it is easily shown that $\langle \eta_0^2 \rangle = \langle \eta_1^2 \rangle = \langle \eta_2^2 \rangle \approx 2(D_{\text{eff}}/\ell^2)t$ in the large t limit where

$$D_{\text{eff}}(2) = \ell^2 \left[\frac{\alpha^2 D_0 + 2(\frac{\kappa}{\gamma})^2 \bar{D}_1}{2(\alpha + 2\frac{\kappa}{\gamma})^2} \right]. \quad (34)$$

For both $N = 1$ and $N = 2$, the variance shows diffusive behaviour in the long-time limit. For a general N motor system, we therefore expect $\langle \eta_i^2 \rangle \sim 2(D_{\text{eff}}/\ell^2)t$, where D_{eff} is the effective diffusion coefficient of the motor-cargo assembly. Based on a simple extrapolation of the analytical results for $N = 1$ and $N = 2$, we conjecture eq.21 as the effective diffusion coefficient for arbitrary N .

References

1. J. Howard, *Mechanics of Motor Proteins and Cytoskeleton*, (Sinauer Press, Sunderland, MA, 2001).
2. A. B. Kolomeisky, *Motor Proteins and Molecular Motors*, (CRC Press, Boca Raton, FL, 2015).
3. D. Chowdhury, Phys. Rep. **529**, (2013) 1.
4. A. Desai and T. J. Mitchison, Ann. Rev. Cell. Dev. Biol. **13**, (1997) 83.
5. S. M. Block and L. S. B. Goldstein and B. J. Schnapp, Nature **348** (1990), 348.
6. S. P. Gross, Curr. Biol. **17**, (2007) R478.
7. S. P. Gross, Phys. Biol. **1**, (2004) R1.
8. M. A. Welte, Curr. Biol. **14**, (2004) R525.
9. V. Soppina, A. K. Rai, A. J. Ramaiya, P. Barak and R. Mallik, Proc. Natl. Acad. Sci. USA **106**, (2009) 19381.
10. A. G. Hendricks, E. Perlson, J. L. Ross, H. W. Schroeder III, M. Takito and E. L. F. Holzbaur, Curr. Biol. **20**, (2010) 697.
11. A. R. Rogers, J. W. Driver, P. E. Constantinou, D. K. Jamisonb and M. R. Diehl, Phys. Chem. Chem. Phys. **11**, (2009) 4882.
12. K. Furuta, A. Furuta, Y. Y. Toyoshima, M. Amino, K. Oiwa and H. Kojima, Proc. Natl. Acad. Sci. USA **110**, (2013) 501.
13. C. M. Coppin, J. T. Finer, J. A. Spudich and R. D. Vale, Proc. Natl. Acad. Sci. USA **93**, (1996) 1913.
14. C. M. Coppin, D. W. Pierce, L. O. Hsu and R. D. Vale, Proc. Natl. Acad. Sci. USA **94**, (1997) 8539.
15. S. Klumpp and R. Lipowsky, Proc. Natl. Acad. Sci. USA **102**, (2005) 17284.

16. M. J. Müller, S. Klumpp and R. Lipowsky, Proc. Natl. Acad. Sci. USA **105**, (2008) 4609.
17. M. J. I. Müller and S. Klumpp and R. Lipowsky, Biophys. J. **98**, (2010) 2610.
18. M. J. I. Müller and S. Klumpp and R. Lipowsky, J. Stat. Phys. **133**, (2008) 1059.
19. A. Kunwar, S. K. Tripathy, J. Xu, M. K. Mattson, P. Anand, R. Sigua, M. Vershinin, R. J. McKenney, C. C. Yu, A. Mogilner and S. P. Gross, Proc. Natl. Acad. Sci. USA **108**, (2011) 18960.
20. A. Kunwar, M. Vershinin, J Xu and S P Gross, Curr. Biol. **18**, (2008) 1173.
21. D. Materassi, S. Roychowdhury, T. Hays and M. Salapaka, BMC Biophys. **6**, (2013) 14.
22. S. Bouzat and F. Falo, Phys. Biol. **7**, (2010) 046009.
23. S. Bouzat and F. Falo, Phys. Biol. **8**, (2011) 066010.
24. J. W. Driver, A. R. Rogers, D. K. Jaminson, R. K. Das, A. B. Kolomeisky and M. R. Diehl, Phys. Chem. Chem. Phys. **12**, (2012) 10398.
25. F. Berger, C. Keller, S. Klumpp, and R. Lipowsky, Phys. Rev. Lett. **108**, (2012) 208101.
26. F. Berger, C. Keller, R. Lipowsky and S. Klumpp, Cell. Molec. Bioeng. **6**, (2013) 48.
27. F. Berger, C. Keller, S. Klumpp and R. Lipowsky, Phys. Rev. E **91**, (2015) 022701.
28. E. Zimmermann and U. Seifert, Phys. Rev. E **91**, (2015) 022709.
29. S. Bouzat, Phys. Rev. E **93**, (2016) 012401.
30. R. Mallik, B. C. Carter, S. A. Lex, S. J. King and S. P. Gross, Nature **427**, (2004) 649.
31. A. K. Rai and A. Rai and A. J. Ramaiya and R. Jha and R. Mallik, Cell **152**, (2013) 1.
32. N. G. van Kampen, *Stochastic Processes in Physics and Chemistry* (Elsevier, Amsterdam, 2007).
33. M. E. Fisher and A. B. Kolomeisky, Proc. Natl. Acad. Sci. USA **96**, (1999) 6597.
34. T. Schmiedl and U. Seifert, Eur. Phys. Lett. **83**, (2008) 30005.
35. E. B. Stukalin, H. Phillips III and A. B. Kolomeisky, Phys. Rev. Lett. **94**, (2005) 238101.
36. E. B. Stukalin and A. B. Kolomeisky, Phys. Rev. E **73**, (2006) 031922.
37. K. Visscher, M. J. Schnitzer and S. M. Block, Nature **400**, (1999) 184.

